Parallel plate waveguide with anisotropic graphene plates: Effect of electric and magnetic biases

Ali Malekabadi,[1,a)] Serge A. Charlebois,[1,b)] and Dominic Deslandes[2,c)]
[1]*Department of Electrical and Computer Engineering, University of Sherbrooke, Quebec, Canada*
[2]*Department of Electrical and Computer Engineering, University of Quebec at Montreal, Quebec, Canada*

(Received 17 December 2012; accepted 21 January 2013; published online 18 March 2013)

The performances of a parallel plate waveguide (PPWG) supported by perfect electric conductor (PEC)-graphene and graphene-graphene plates are evaluated. The graphene plate behavior is modeled as an anisotropic medium with both diagonal and Hall conductivities derived from Kubo formula. The PPWG modes supported by PEC-graphene and graphene-graphene plates are studied. Maxwell's equations are solved for these two waveguides, while the graphene layers are biased with an electric field only and with both electric and magnetic fields. It is shown that when both electric and magnetic biases are applied to the graphene, a hybrid mode (simultaneous transverse electric (TE) and transverse magnetic (TM) modes) will propagate inside the waveguide. The intensity of each TE and TM modes can be adjusted with the applied external bias fields. Study of different waveguides demonstrates that by decreasing the plate separation (d), the wave confinement improves. However, it increases the waveguide attenuation. A dielectric layer inserted between the plates can also be used to improve the wave confinement. The presented analytical procedure is applicable to other guiding structures having walls with isotropic or anisotropic conductivities. © *2013 American Institute of Physics*. [http://dx.doi.org/10.1063/1.4794169]

I. INTRODUCTION

Although it was not expected to exist in nature, a two-dimensional (2D) atomic layer of carbon was experimentally discovered in 2004. Novoselov *et al*., have demonstrated that a few layers of graphene behave like a conductor and are stable under ambient conditions.[1] With a thickness of 0.34 nm, this 2D honeycomb lattice of carbon atoms demonstrates promising properties such as high carrier mobility, thus, opening a new window to high-speed nano-electronics. Other 2D atomic crystals were investigated, and their electronic properties were compared with graphene in Ref. 3.

Electric field effect experiments on graphene reveal an ambipolar behavior similar to that observed in semiconductors.[1] The charge carrier density can be tuned continuously between electrons and holes[2,4] thus enabling a control on the electronic properties of graphene by applying an external voltage. The carrier concentration can reach as much as $10^{13}\,cm^{-2}$, and the mobility of both electrons and holes can exceed 15 000 $cm^2\,V^{-1}\,s^{-1}$, even under ambient conditions.[2] Also, the mobility can reach 100,000 $cm^2\,V^{-1}\,s^{-1}$ under certain conditions.[2] It is now generally accepted that these distinctive properties of graphene can be explained using a relativistic gapless semiconductor model using the Dirac equation.[4]

In early papers, graphene samples were prepared by mechanical exfoliation of graphite crystals using adhesive tape.[1–4] The main problem of this technique was the limited achievable size, in the order of 10 μm.[1] Using chemical vapor deposition methods, it is now possible to synthesize large-area graphene layers on the order of a few square centimeters.[5] These graphene films can be transferred from their growth substrate (e.g., copper) to arbitrary materials such as silicon dioxide, polymer films, or metallic grids (in order to have suspended graphene).

Microwave applications of graphene layers have not yet been extensively explored, mainly due to the small size of the layers available until recently. Nevertheless, due to their unique properties, there is a substantial interest in applying them to design novel electronic and photonic devices.[8,9] For comparison, carbon nanotubes (CNTs) have a high input impedance (in the range of 20 kΩ up to 10 MΩ) resulting in a huge mismatch with any other devices or circuits (with standard impedance of 50 or 75 Ω).[6] Unlike the CNTs, the possibility to control the graphene conductivity (impedance) by the field effect makes it more applicable for microwave and RF applications.[6] This behavior was studied by printing a coplanar waveguide (CPW) over a graphene layer. By applying an external voltage (between the central line and the ground electrodes), the transmission characteristics of CPWs (S11 and S12) were measured up to 7 GHz in Ref. 6, up to 60 GHz in Ref. 7, and up to 110 GHz in Refs. 10 and 11. Furthermore, Hanson studied the interaction of an electromagnetic current source in the neighborhood of a voltage biased graphene layer.[12] It was demonstrated that surface wave propagation can be controlled by varying the graphene conductivity with the applied voltage.[12] Hanson also performed the same investigation with magnetically biased graphene layers[13] The electromagnetic wave propagation inside graphene based parallel plate waveguide (PPWG) was investigated in Ref. 14 under the assumption that the graphene layers were only biased with electrostatic fields. It was shown that quasi-TEM modes can propagate inside the graphene waveguide with attenuation similar to structures enclosed by thin metal plates, and also the voltage bias provides some

[a)]E-mail: seyed.ali.malek.abadi@usherbrooke.ca.
[b)]E-mail: serge.charlebois@usherbrooke.ca.
[c)]E-mail: deslandes.dominic@uqam.ca.

control over the propagation.[12] Gusynin *et al.* published a thorough study of the magneto-optical conductivity of graphene.[17–19] They show that under magnetic field bias, the conductivity of graphene can be modeled by a tensor with diagonal elements linked to the Hall effect.[17] This provides further control over the electromagnetic wave propagation in graphene structures.

This paper presents a comprehensive study of PPWG enclosed by anisotropic graphene plates. Based on the preliminary results reported in Ref. 16, the graphene is modeled with a conductivity tensor as presented in Ref. 13 (Sec. II). The effect of external electric and magnetic fields on this tensor is investigated. In Sec. III, two PPWGs with perfect electric conductor (PEC)-graphene and graphene-graphene walls are studied, using this conductivity tensor. Maxwell's equations are solved considering either only an electric field bias or both electric and magnetic fields. In each case, the dispersion equation and propagating modes are derived and discussed. The PPWG design with electrically biased graphene walls, which has been studied in Ref. 14, is presented here to show the validity of our analytical derivation (as a special case of our presented results). It is shown that a hybrid mode propagates in graphene PPWGs with both electric and magnetic bias fields. The power density of each transverse electric (TE) and transverse magnetic (TM) modes can be adjusted with the applied external bias fields. This phenomenon enables a variety of application in microwave and terahertz frequency bands. Study of different waveguides demonstrates that by decreasing the plate separation (d), the wave confinement improves. However, it increases the waveguide attenuation. Two other techniques are also discussed to improve the confinement of the electromagnetic field: the insertion of a dielectric layer between the plates and an increase of the graphene conductivity by increasing the static electric fields. The presented analytical techniques can also be used to study other guiding structures enclosed by walls with isotropic or anisotropic conductivities.

II. GRAPHENE MODEL

A. DC properties

As highlighted in Sec. I, charge carrier density in graphene can be varied continuously. Concerning the experimental results of the electric field effect on graphene sheets (the conductivity σ versus the gate voltage V_G, see Fig. 3 in Ref. 1), one can observe that the conductivity σ is proportional to V_G. Employing the semi-classical Drude model, it is possible to describe the electrical conductivity with $\sigma = n_s e\mu$, in which n_s is the carrier density, μ the carrier mobility, and e the charge quanta. Considering the ground plate (gate) and graphene as a parallel plate capacitor, the density is found to behave as $n_s = \varepsilon_r\varepsilon_0 V_G/de$, where ε_r and ε_0 are the dielectric and vacuum permittivity, respectively, and d is the thickness of the dielectric separating the gate and the graphene layer. The experimental results presented in Ref. 4 using a Hall bar configuration to measure the Hall coefficient $R_H = 1/n_s e$ gives $n_s/V_G = 7.3 \times 10^{10}$ cm^{-2} V^{-1} and $\mu = 1.5 \times 10^4$ cm^2 V^{-1} s^{-1} for both electrons and holes. A comparison between the electrical properties of graphene and copper is provided in Table I. As it can be observed from this table, although the graphene mobility is about 400 times greater than that of copper, the graphene's conductivity is poor in comparison with the conductivity of copper due to the lack of carriers. By increasing the gate voltage, the conductivity will rise and by applying a magnetic field perpendicular to the graphene surface, the Hall conductivity will increase. We note that the properties of graphene, such as the carrier density and mobility and the position of the Dirac point, are highly sensitive to temperature and to the substrate used. For references, the properties of graphene have been investigated over a variety of substrates like SiO_2 (Refs. 1 and 2), SiC (Ref. 23), metal plates (Ref. 24), mica (Ref. 25), and hexagonal boron nitride (BN).[26]

TABLE I. Comparison between graphene and copper conductivities (DC).

		Graphene	
	Copper[a]	$V_g = 0$	$V_g = 100$
n_s (cm^{-2})	4.36×10^{19}	3×10^{11}	3×10^{13}
μ (cm^{2}V^{-1}s^{-1})	2.32×10^{1}	1×10^{4}	1×10^{4}
σ (S)	1.62×10^{2}	4.8×10^{-4}	4.8×10^{-2}

[a]We consider a monolayer of copper.

B. AC properties

Due to the massless Dirac fermion nature of its quasiparticles, the diagonal and Hall conductivity tensors of the graphene demonstrate unusual characteristics.[18,19] We calculated the AC conductivities of graphene using the Kubo formula, which is based on the Dirac equation. We present here in SI units the diagonal conductivity[13,18]

$$\sigma_d(\mu_c(E_o), B_o) = \frac{e^2 v_F^2 |eB_0|(\omega - j2\Gamma)\hbar}{-j\pi} \times \sum_{n=0}^{\infty} \left\{ \frac{n_F(M_n) - n_F(M_{n+1}) + n_F(-M_{n+1}) - n_F(-M_n)}{(M_{n+1} - M_n)^2 - (\omega - j2\Gamma)^2\hbar^2} \times \left(1 - \frac{\Delta^2}{M_n M_{n+1}}\right) \frac{1}{M_{n+1} - M_n} \right.$$
$$\left. + \frac{n_F(-M_n) - n_F(M_{n+1}) + n_F(-M_{n+1}) - n_F(M_n)}{(M_{n+1} + M_n)^2 - (\omega - j2\Gamma)^2\hbar} \times \left(1 + \frac{\Delta^2}{M_n M_{n+1}}\right) \frac{1}{M_{n+1} + M_n} \right\}, \quad (1)$$

and the Hall conductivity (off diagonal element)

$$\sigma_h(\mu_c(E_0),B_0) = -\frac{e^2 v_F^2 eB_0}{\pi}\sum_{n=0}^{\infty}\{n_F(M_n) - n_F(M_{n+1}) - n_F(-M_{n+1}) + n_F(-M_n)\}$$
$$\times\left\{\left(1-\frac{\Delta^2}{M_nM_{n+1}}\right)\frac{1}{(M_{n+1}-M_n)^2-(\omega-j2\Gamma)^2\hbar^2} + \left(1+\frac{\Delta^2}{M_nM_{n+1}}\right)\frac{1}{(M_{n+1}+M_n)^2-(\omega-j2\Gamma)^2\hbar^2}\right\}, \quad (2)$$

where $M_n = \sqrt{\Delta^2 + 2n_s v_F^2 |eB_0|\hbar}$ is the energy of the Landau level, which includes the excitonic gap Δ. Also, Γ is the scattering rate independent on Landau levels, $v_f = 10^6$m/s is the Fermi velocity, $\hbar$ is the reduced Planck's constant, B_0 is the external magnetic field bias, n_F is the Fermi-Dirac distribution $n_F(\omega) = 1/(e^{-(\omega-\mu_c)/k_BT}+1)$, k_B is Boltzmann's constant, μ_c is the chemical potential, and T is the temperature.

The chemical potential μ_c is obtained from the electric field bias E_0 with the following equations:[13]

$$E_0 = \frac{e}{\pi\varepsilon_0\hbar^2 v_F^2}\int_0^{\infty}\varepsilon(n_F(\varepsilon-\mu_c) - n_F(\varepsilon+\mu_c))d\varepsilon, \quad (3)$$

where the integral is performed on all relevant energies ε. As discussed before, the electric field bias E_0 changes the carrier density of the graphene sheet. The chemical potential obtained from Eq. (3) provides the means to take into account the carrier density in the Kubo formalism that leads to Eqs. (1) and (2). Equation (3) is depicted in Fig. 2 of Ref. 13.

In Secs. III A and III B of this paper, it is assumed that the graphene layer has chemical potential of $\mu_c = 0.2$ eV (which is provided by $V_G = 100$ V for a 100 nm thick dielectric), the scattering rate of $\Gamma = 1/\tau = 1.3$ meV ($\tau = 0.5$ ps, corresponding to a mean free path of several hundred nanometers)[15] there is no excitonic gap energy Δ and T = 300 K.

III. PARALLEL PLATE WAVEGUIDE

A. PEC-graphene plates

Fig. 1 shows the analyzed PPWG. In this structure, the plate, which is placed at $y = 0$, is assumed to be a PEC ($\sigma \to \infty$) and the other one, which is located at $y = d$, is assumed to be a graphene sheet. The graphene layer is biased with uniform and time constant external electric field E_0 and magnetic field B_0. The electric field is provided by applying gate voltage V_G between the graphene sheet and the PEC through DC contacts. As one possible implementation, the magnetic field B_0 could be provided by a large magnet placed below the PEC. The biased graphene plate is modeled by a conductivity tensor, as in Eq. (7), in which both the diagonal and Hall conductivities can be tuned with the applied fields. The external electric and magnetic fields are oriented along the y axis. The distance between the plates is equal to d and the wave is propagating toward the z axis. The mediums above the graphene sheet, between the two plates and under the PEC plates, are named I, II, and III, respectively. The permittivity and permeability of mediums I, II, and III are labeled $\varepsilon_1, \mu_1, \varepsilon_2, \mu_2$, and ε_3, μ_3, respectively.

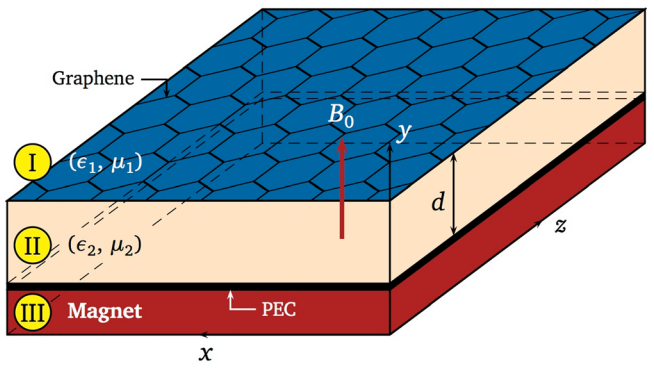

FIG. 1. The PPWG supported by PEC and graphene plates (cross section view). The graphene layer is biased with electric and magnetic fields. The electric field is provided by applying a gate voltage V_G between the graphene and PEC plates and the magnetic field B_0 is considered uniform (brought by an external magnet placed below the PEC as illustrated here). The distance between the plates is assumed to be d.

In conventional PPWG systems, it is customary to divide the electromagnetic field into two "groups" linked to the TE and TM modes. However, due to the existence of the Hall effect, which is the result of the presence of the magnetic field, the boundary conditions cannot be satisfied assuming TE or TM mode separately. Due to the tensor nature of the conductivity in graphene, the z component of the electric field (assuming TM mode only) splits into two, x and z components (see boundary condition in (7)), where the x component is in contrast with TM mode assumption. This phenomenon is analogue to the Faraday rotation,[21,22] where the incident wave's polarization rotates according to the magnetic bias field magnitude and the incident angle. In order to satisfy the boundary conditions, it is therefore necessary to consider both TE and TM modes simultaneously. Thus, starting from Maxwell Equations, one can rewrite the x and y components of the electric and magnetic fields in terms of their z components

$$\begin{cases} E_x = \dfrac{-j}{k_{c(m)}^2}\left(\beta\dfrac{\partial E_z}{\partial x} + \omega\mu_m\dfrac{\partial H_z}{\partial y}\right) \\ E_y = \dfrac{j}{k_{c(m)}^2}\left(-\beta\dfrac{\partial E_z}{\partial y} + \omega\mu_m\dfrac{\partial H_z}{\partial x}\right) \\ H_x = \dfrac{j}{k_{c(m)}^2}\left(\omega\varepsilon_m\dfrac{\partial E_z}{\partial y} - \beta\dfrac{\partial H_z}{\partial x}\right) \\ H_y = \dfrac{-j}{k_{c(m)}^2}\left(\omega\varepsilon_m\dfrac{\partial E_z}{\partial x} - \beta\dfrac{\partial H_z}{\partial y}\right) \end{cases}, \quad (4)$$

where $k_{c(m)}^2 = k_m^2 - \beta^2$ is the cutoff wavenumber, k_m is the wavenumber, and $m = 1, 2$ for the mediums I and II.[20] The propagation constant, β, is assumed to be the same in regions I and II providing the phase matching of the fields along the border at y = d. In order to obtain the transverse electric (E_z)

and magnetic (H_z) fields, one solves the wave equation in region II, resulting in

$$\begin{cases} e_{z(2)} = B_1 \sin k_{c(2)} \mathrm{y} \\ h_{z(2)} = B_2 \cos k_{c(2)} \mathrm{y} \end{cases}, \tag{5}$$

where $E_{z(2)} = e_{z(2)} e^{-j\beta z}$ and $H_{z(2)} = h_{z(2)} e^{-j\beta z}$. Also note that the cosine part of $e_{z(2)}$ is set to zero according to the fact that the electric field should vanish at the PEC surface. Also, the sine part of $h_{z(2)}$ should be zero because $e_{x(2)}$ at the PEC border is equal to zero. Using Eq. (4), all the other components of the electric and magnetic fields can be derived. The same procedure is used to evaluate the electromagnetic fields in region I. However, in this region, the $e_{z(1)}$ and $h_{z(1)}$ should vanish, while $\mathrm{y} \to \infty$. Thus, the z components of the electric and magnetic fields in this region are derived by solving the wave equation

$$\begin{cases} e_{z(1)} = A_1 e^{-jk_{c(1)}y} \\ h_{z(1)} = A_2 e^{-jk_{c(1)}y} \end{cases}. \tag{6}$$

Note that A_1, A_2, B_1, B_2, and β are unknowns. As the next step, the boundary conditions at $y = d$ are applied to the electromagnetic fields derived above. The tensor for the conductivity leads to boundary conditions (for x and z components) expressed as

$$\begin{cases} (\bar{E}_2 - \bar{E}_1) \times (-\hat{y}) = 0 \\ \hat{n} \times (\bar{H}_2 - \bar{H}_1) = \bar{J}_s = \begin{pmatrix} J_{sz} \\ J_{sx} \end{pmatrix} = \begin{pmatrix} \sigma_d & \pm\sigma_h \\ \mp\sigma_h & \sigma_d \end{pmatrix} \cdot \begin{pmatrix} e_{z(2)} \\ e_{x(2)} \end{pmatrix} \end{cases}, \tag{7}$$

where σ_d and σ_h are the diagonal and Hall electrical conductivities, respectively, from Eqs. (1) and (2). The top (bottom) sign of the off diagonal elements is used when the B_0 field is in the positive (negative) y direction and is related to the carrier motion. For example, the x component of the surface current J_{sx} is the sum of the product of the diagonal conductivity with $e_{x(2)}$ and the Hall conductivity with $e_{z(2)}$. Each of the boundary conditions (7) is divided into two parts (x and z components) and will result into four equations in which A_1, A_2, B_1, B_2, and β are the unknowns. For nontrivial solution, the determinant of the two above equations must vanish, leading to the dispersion equation which is

$$\left[\cot(k_{c(2)}d) + j\left(\frac{k_{c(1)}}{k_{c(2)}}\frac{\mu_2}{\mu_1} + \frac{\sigma_d \omega \mu_2}{k_{c(2)}}\right)\right] \times \left[\cot(k_{c(2)}d) + j\left(\frac{k_{c(2)}}{k_{c(1)}}\frac{\varepsilon_1}{\varepsilon_2} + \frac{k_{c(2)}\sigma_d}{\omega\varepsilon_2}\right)\right] - (\sigma_h \eta_2)^2 = 0. \tag{8}$$

Using the definition of $k_{c(1)}$ and $k_{c(2)}$, the roots of the dispersion equation (8) will give the values of β_p (the propagation constant of the p_{th} mode) as a function of the frequency. As a first case, one could remove the magnetic bias letting the Hall conductivity vanish, $\sigma_h = 0$, in this equation. The PPWG, therefore, consists of one PEC wall and a second wall made of a few nanometer thick finite conductivity metal. In this situation, the dispersion equation will reduce to Eqs. (9a) and (9b), which represent dispersion relations for the TE and the TM modes, respectively. The fact that the graphene conductivity can be varied by an electric field bias provides control on the roots of these equations

$$\cot(k_{c(2)}d) + j\left(\frac{k_{c(1)}}{k_{c(2)}}\frac{\mu_2}{\mu_1} + \frac{\sigma_d \omega \mu_2}{k_{c(2)}}\right) = 0, \tag{9a}$$

$$\cot(k_{c(2)}d) + j\left(\frac{k_{c(2)}}{k_{c(1)}}\frac{\varepsilon_1}{\varepsilon_2} + \frac{k_{c(2)}\sigma_d}{\omega\varepsilon_2}\right) = 0. \tag{9b}$$

The PPWG behavior can thus be continuously tuned from non-guiding if $\sigma_d \to 0$ to a PEC-PEC PPWG, when $\sigma_d \to \infty$. In the latter case, we get the textbook solution $k_{c(2)} = n\pi/d$ (e.g., Ref. 20). Also, Eq. (9b) is the same as Eq. (9) in Ref. 14, when $\sigma_b \to \infty$ (as defined in Ref. 14). Moreover, letting $\sigma_d, \sigma_h \to \infty$ gives dispersion relations for dielectric coated conductor waveguide.[28]

To compare the graphene based PPWG with one using a normal metal, one can use the Drude model for the conductivity needed in Eq. (9). In the case of a very thin metal layers, we use the Drude-Smith model, which is experimentally verified in far-infrared spectral region from 0.2 to 2.7 THz.

$$\sigma(\omega) = \frac{\varepsilon_0 \omega_p^2 \tau}{1 + j\omega\tau}\left(1 + \frac{c}{1 + j\omega\tau}\right), \tag{10}$$

where ω_p, τ, and c are the plasma frequency, scattering time, and the persistence of velocity, respectively.[27] For a 4 nm thick gold layer, the plasma frequency, $\omega_p/2\pi$, is 280 THz, scattering time, τ, is 18 fs, and the persistence of velocity, c, is -1 (Ref. 27). Fig. 2 shows the real and imaginary parts of the propagation constant in PEC-graphene (for plate separations of 100 μm, 100 nm, and 10 nm) and PEC-conductor with $\sigma = 1$ s/m (for plate separation of 100 μm) for different modes in the absence of the magnetic field. In the case of PEC-gold plates, due to $\sigma_d \omega \mu_2 / k_{c(2)}$, $k_{c(2)}\sigma_d/\omega\varepsilon_2 \gg 1$ (by assuming the free space condition for regions I and II in Eq. (9), we have $k_{c1}\mu_2/k_{c2}\mu_1 = k_{c2}\varepsilon_1/k_{c1}\varepsilon_2 = 1$), the propagation constant is approximately the same as PEC-PEC situation. Moreover, assuming a conductor with $\sigma = 1$ s/m at $y = d$, the results for the propagation constant are similar to a PEC-PEC structure. Thus, for a 4 nm thick gold layer, with a minimum conductivity of 6.1×10^5 s/m in the 0.2 to 2.7 THz frequency range, the propagation constant is almost the same as a PEC-PEC structure.

In the case of PEC-graphene, with $\mathrm{d} = 100$ μm (see Figs. 2(a) and 2(b)), although the imaginary part of the slow-wave factor (SWF), β/k_0 is almost zero for frequencies above 0.4 THz, implying low loss propagation, the real part of the SWF is around 1, representing a low confinement capability of the waveguide. This is due to the fact that $\beta/k_0 = \sqrt{\varepsilon_{re}} = n_e$ should be greater than 1 to give fiber optic like propagation in PPWG.

Different solutions can be implemented to increase the SWF, such as increasing graphene conductivity, using a

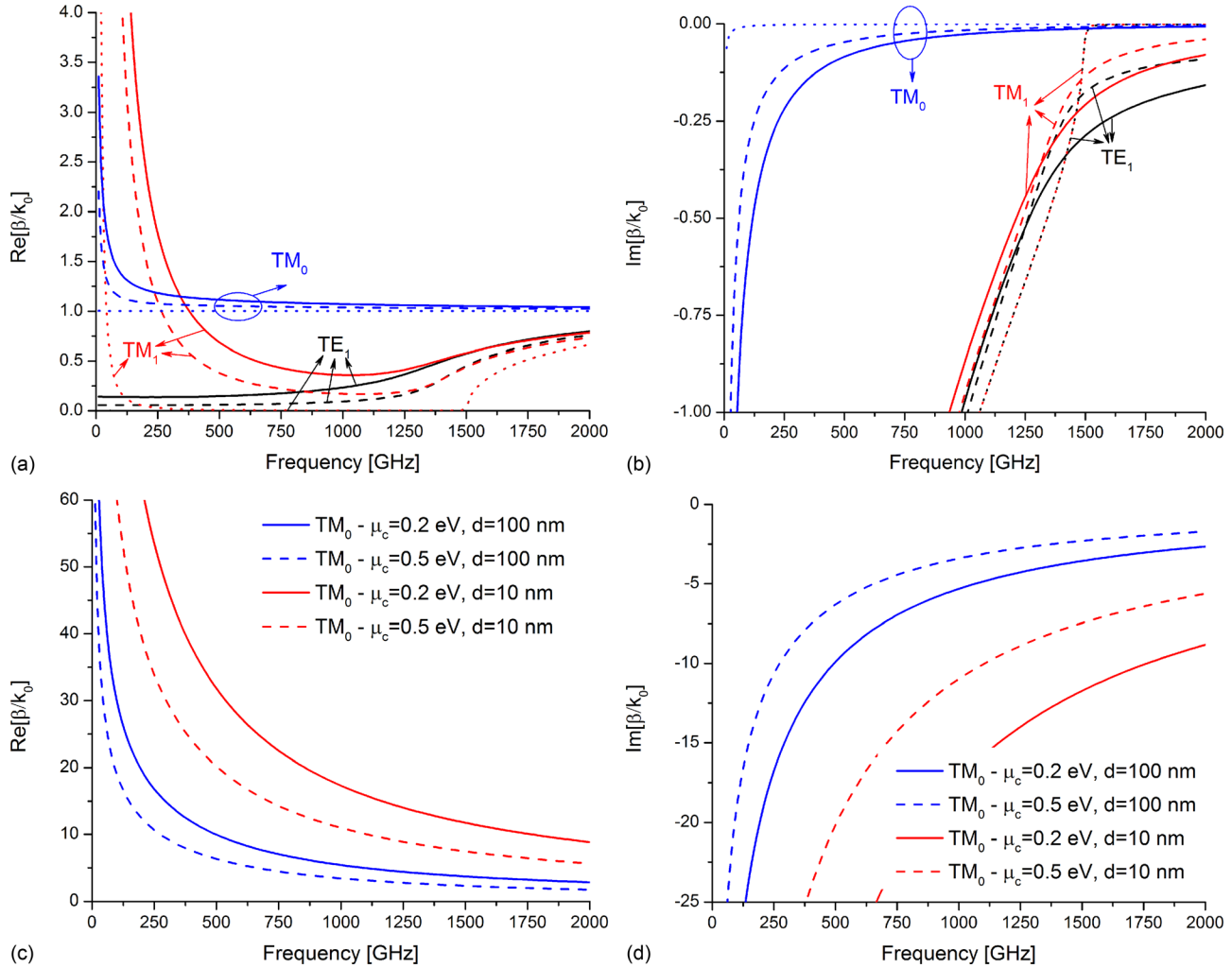

FIG. 2. The real and imaginary parts of the propagation constant of PEC-graphene and PEC-conductor ($\sigma = 1$ s/m) PPWGs. (a) and (b) first three modes (TM_0, TM_1, and TE_1) for the plate separation of 100 μm (solid line: $\mu_c = 0.2$ eV, dashed line: $\mu_c = 0.5$ eV, and dots: conductor with $\sigma = 1$ s/m). (c) and (d) first mode (TM_0) for the plate separation of 10 nm and 100 nm. All in the absence of the external magnetic field $B_0 = 0 \rightarrow \sigma_h = 0$.

dielectric in region II, and decreasing the plate separation d. Increasing graphene conductivity is possible by applying a stronger electric field between the graphene and the ground plane. However, it suffers from possible current leakage under high voltage. Inserting a dielectric material between the graphene and the ground plane makes the waveguide behavior more similar to a dielectric image waveguide, which is not subject of this paper. However, one can investigate the properties of this waveguide based on the presented dispersion equation (8) and (9). Decreasing the plate separation will shift the cutoff frequency of TE_n and TM_n modes ($f_c = 1/2d\sqrt{\mu\varepsilon}$), but, it will not affect the TM_0 mode (here quasi-TEM in PEC-graphene PPWG), which is the mode of interest. Therefore, in Fig. 2, we present the propagation constant of the PEC-graphene structure for two other plate separations of 10 nm and 100 nm.

When there is an external magnetic field, both TE and TM modes exist simultaneously (hybrid mode propagation). In order to calculate the phase constant of the propagating wave inside the waveguide, we assume, for simplicity and without loss of generality, the free space condition for both regions I and II. In this case, Eq. (8) reduces to

$$\left[\cot(k_{c0}d) + j\left(1 + \frac{\sigma_d \omega \mu_0}{k_{c0}}\right)\right] \times \left[\cot(k_{c0}d) + j\left(1 + \frac{k_{c0}\sigma_d}{\omega\varepsilon_0}\right)\right] - (\sigma_h \eta_0)^2 = 0, \tag{11}$$

where $k_{c0} = k_{c1} = k_{c2}$. By solving this equation, k_{c0} is derived and then β can be computed. The results are depicted in Fig. 3 for plate separations of d = 100 nm and 10 nm (for TM_0 mode). The attenuation of these waveguides is presented in Table II. The attenuation is derived using $\alpha = 8.686\,\mathrm{Im}(\beta)$, where β is available from solving the dispersion equation. As mentioned before, by increasing the separation between the plates, the imaginary part of the propagation constant will decrease, providing a waveguide with smaller loss. But, at the same time, it will decrease the SWF, resulting in a poor confinement of the field inside the waveguide.

The time average power propagating through a surface area S is derived from the pointing vector, which can be divided in TE and TM contributions as

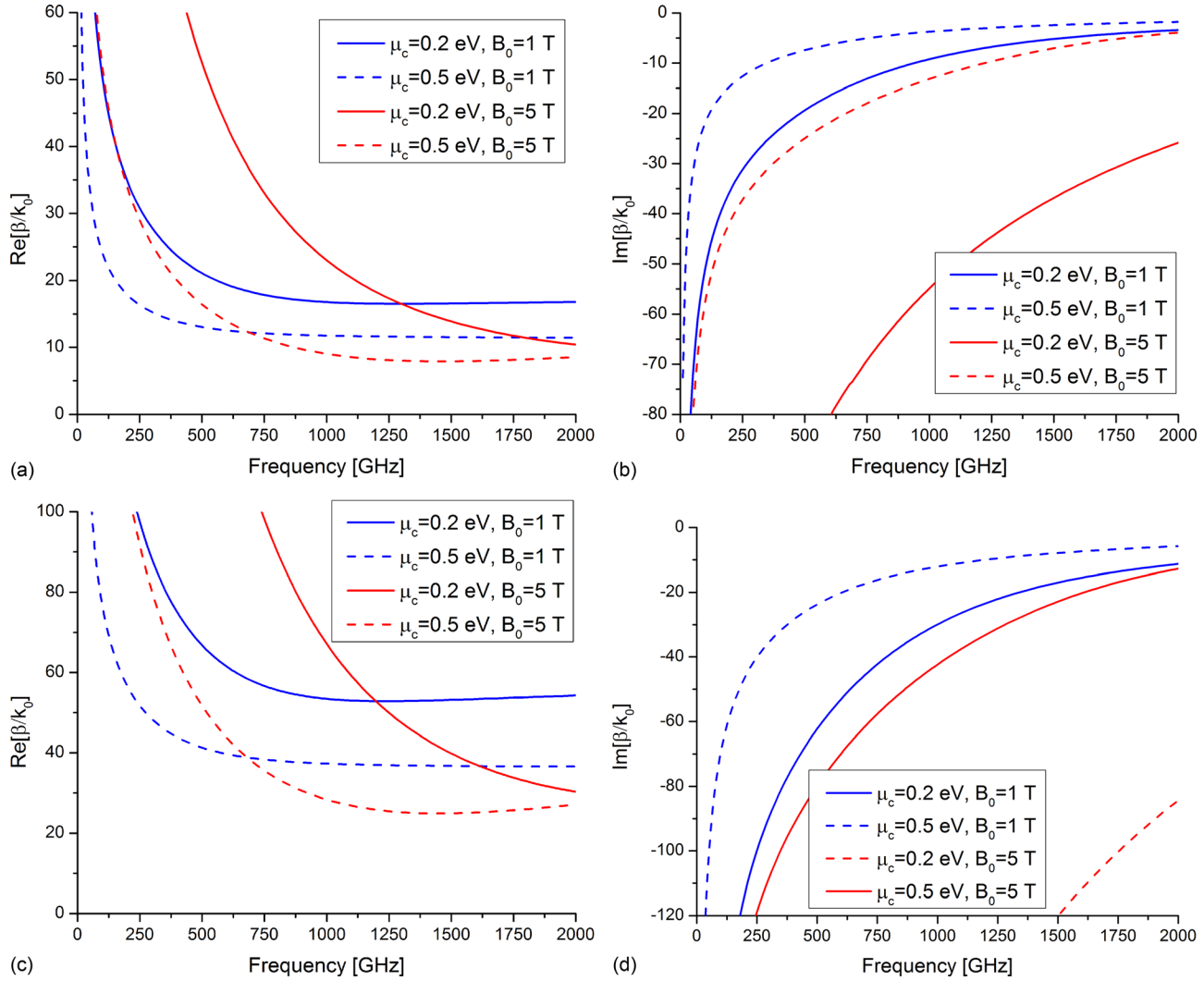

FIG. 3. Real and imaginary-parts of propagation constants of PPWG with PEC-graphene walls. These results are derived by solving Eq. (8). The graphene conductivities derived from Eqs. (1) and (2) assuming $\Gamma = 1.3$ meV. The plate separations are (a) and (b) 100 nm and (c) and (d) 10 nm.

TABLE II. Attenuation (α dB/μm) of PEC-graphene PPWG with d = 100 nm.

f (GHz)		10	100	250	500	750	1000	1500	2000
PEC-Gr $B_0 = 0$	$\mu_c = 0.2$ eV	0.1857	0.544	0.7623	0.9006	0.9488	0.9676	0.9708	0.9634
	$\mu_c = 0.5$ eV	0.1175	0.3447	0.4838	0.5739	0.6063	0.6199	0.6252	0.624
PEC-Gr $B_0 = 1$ T	$\mu_c = 0.2$ eV	0.2947	0.9279	1.4205	1.7630	1.7868	1.6776	1.4137	1.2315
	$\mu_c = 0.5$ eV	0.1322	0.3978	0.5729	0.6744	0.6896	0.6828	0.6597	0.6451
PEC-Gr $B_0 = 5$ T	$\mu_c = 0.2$ eV	1.1129	3.6268	5.9324	8.1896	9.44696	9.9862	10.0569	9.407
	$\mu_c = 0.5$ eV	0.3207	1.0483	1.6930	2.2677	2.4506	2.3939	1.9227	1.4158

$$P_{avg} = \frac{1}{2}\mathrm{Re}\int_S (\bar{E} \times \bar{H}^*).\mathrm{d}\bar{s} = \frac{1}{2}\mathrm{Re}\left(\sum_{m=1}^{3}\left(\int\int_S E_{x(m)}H^*_{y(m)}\mathrm{dydx} + \int\int_S E_{y(m)}H^*_{x(m)}\mathrm{dydx}\right)\right) \triangleq P_{avg(TE)} + P_{avg(TM)}, \quad (12)$$

in which $P_{avg(TE)}$ and $P_{avg(TM)}$ are functions of the electric and magnetic bias fields of the graphene. For the evaluation of the power, one should find the roots of Eq. (8) and by setting one of the unknowns in the boundary conditions, perform the integrals in Eq. (12).

Fig. 4 illustrates the normalized proportion of $P_{avg(TM)}/P_{avg(TE)}$ for a given frequency as a function of the chemical potential (electric bias) and magnetic bias. The blue line considers a variation of the chemical potential from 0.05 to 0.5 eV with the magnetic field equal to $B_0 = 1$ T. The red line assumes a change of the magnetic field from 0 to 5 T, while the chemical voltage is set to $\mu_c = 0.2$ eV. The capability to control the wave propagation characteristics is evident in this figure.

B. Graphene-graphene plates

Let us now consider a situation in which both plates of the PPWG are graphene sheets and are biased with both

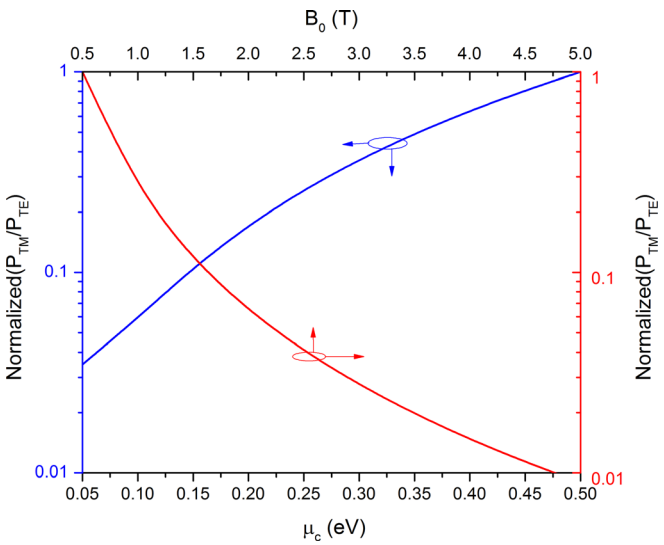

FIG. 4. The proportion of time average power in TE and TM modes for PEC-graphene as a function of the chemical potential (gate voltage V_G) and bias magnetic field at $f = 100$ GHz and for d = 100 nm.

electric and magnetic fields. This waveguide is presented in Fig. 5, where the upper $y = d$ and lower $y = 0$ graphene layers are modeled by independent conductivity tensor elements σ_d, σ_h and σ_d*, σ_h*, respectively. In real experimental systems, the graphene carrier density is known to be non-zero at zero bias. We have voluntarily omitted the biasing scheme that would provide to each graphene film an independent voltage bias. For the sake of simplicity, in the illustration, we have also omitted the components generating the spatially uniform magnetic field. Again, the same procedure as in Sec. III A is applied to study the wave properties inside this waveguide. At first, we solve the wave equation to derive the z components of both electric and magnetic fields in medium II

$$\begin{cases} e_{z(2)} = B_1 \sin k_{c(2)} y + B_2 \cos k_{c(2)} y \\ h_{z(2)} = B_3 \sin k_{c(2)} y + B_4 \cos k_{c(2)} y \end{cases}. \tag{13}$$

In the next step, we calculate other components of the electric and magnetic fields in this medium. Then, the same procedure is performed in the first and third mediums. Finally, we apply the boundary conditions at $y = 0$ and $y = d$ using Eq. (7). From the electric field boundary conditions, it is possible to describe the fields in regions I and III as a function of B_1, B_2, B_3, and B_4. Also, using the magnetic field boundary conditions at $y = 0$, we find that the constants B_2 and B_3 can be expressed in terms of B_1 and B_4. From this and considering the boundary conditions at $y = d$, we can express the dispersion equation as

$$\begin{vmatrix} -\sigma_h \tan(\theta) & -\sigma_h & \tan(\theta) - \mathrm{P} & 1 + \tan(\theta) \times \mathrm{P} \\ \frac{\omega\varepsilon_1}{k_{c(1)}} \times \mathrm{Q}_1 + \sigma_d \tan(\theta) & \frac{\omega\varepsilon_1}{k_{c(1)}} \times \mathrm{Q}_2 + \sigma_d & -\sigma_h \frac{\mathrm{j}\omega\mu_2}{k_{c(2)}} & \sigma_h \frac{\mathrm{j}\omega\mu_2}{k_{c(2)}} \tan(\theta) \\ -\sigma_h^* \tan(\theta) & \sigma_h^* & -\tan(\theta) + \mathrm{P}^* & 1 + \tan(\theta) \times \mathrm{P}^* \\ \frac{\omega\varepsilon_3}{k_{c(3)}} \times \mathrm{Q}_1^* + \sigma_d^* \tan(\theta) & -\frac{\omega\varepsilon_3}{k_{c(3)}} \times \mathrm{Q}_2^* - \sigma_d^* & \sigma_h^* \frac{\mathrm{j}\omega\mu_2}{k_{c(2)}} & \sigma_h^* \frac{\mathrm{j}\omega\mu_2}{k_{c(2)}} \tan(\theta) \end{vmatrix} = 0, \tag{14}$$

in which

$$\begin{aligned} \mathrm{P} &= \mathrm{j}\frac{\omega\mu_2}{k_{c(2)}}\sigma_d + \mathrm{j}\frac{k_{c(1)}}{k_{c(2)}}\frac{\mu_2}{\mu_1}, \\ \mathrm{P}^* &= \mathrm{j}\frac{\omega\mu_2}{k_{c(2)}}\sigma_d^* + \mathrm{j}\frac{k_{c(3)}}{k_{c(2)}}\frac{\mu_2}{\mu_3}, \\ \mathrm{Q}_1 &= \tan(\theta) - \mathrm{j}\frac{k_{c(1)}}{k_{c(2)}}\frac{\varepsilon_2}{\varepsilon_1}, \\ \mathrm{Q}_2 &= 1 + \mathrm{j}\frac{k_{c(1)}}{k_{c(2)}}\frac{\varepsilon_2}{\varepsilon_1}\tan(\theta), \\ \mathrm{Q}_1^* &= \tan(\theta) - \mathrm{j}\frac{k_{c(3)}}{k_{c(2)}}\frac{\varepsilon_2}{\varepsilon_3}, \\ \mathrm{Q}_2^* &= 1 + \mathrm{j}\frac{k_{c(3)}}{k_{c(2)}}\frac{\varepsilon_2}{\varepsilon_3}\tan(\theta). \end{aligned} \tag{15}$$

Our analytical work is partly confirmed by letting $\sigma_h,\ \sigma_h^* \to 0$ (absence of magnetic field bias) in Eq. (14) thus obtaining the same result as Hanson (Eq. (9) in Ref. 14). Also, letting σ_h, σ_h^*, σ_d, and σ_d^* to zero will result in the dispersion equation of the dielectric waveguide.[28] Also, by letting σ_h to zero and changing σ_d to that obtained from the Drude-Smith model, we can analyze PPWGs with a non-ideal conductor instead of a PEC (as done in Sec. III).

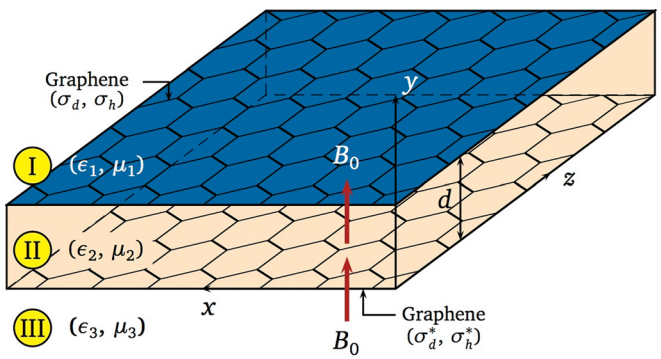

FIG. 5. The PPWG supported by graphene plates (y-z plane). The graphene layers are biased with electric and magnetic fields.

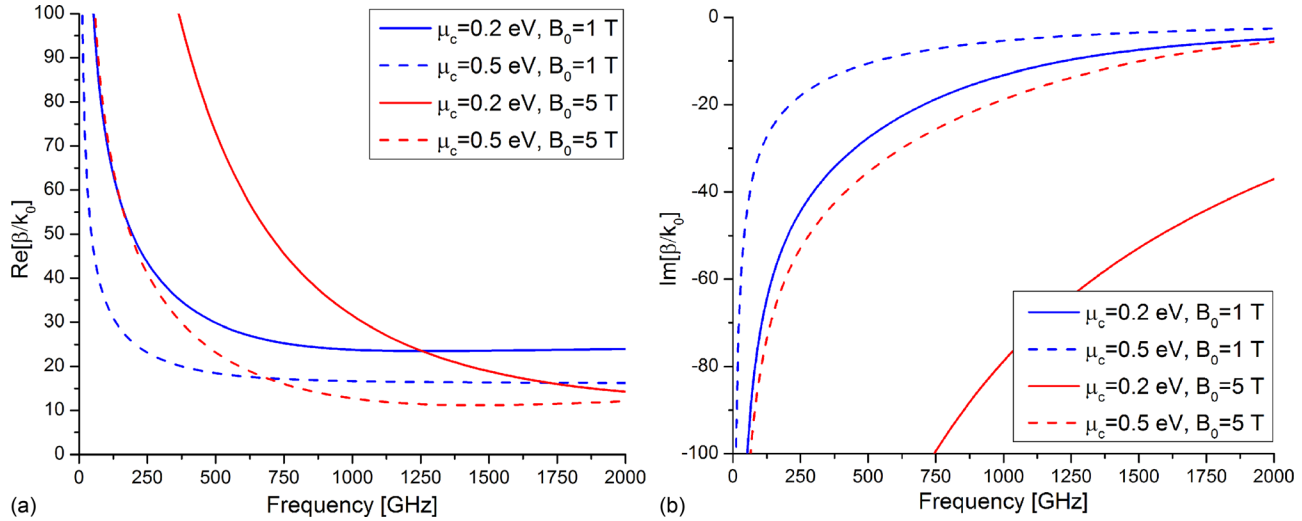

FIG. 6. Real and imaginary-parts of propagation constants of PPWG with graphene-graphene walls. These results are derived from solving Eq. (14). The graphene conductivities derived from Eqs. (1) and (2) assuming $\Gamma = 1.3$ meV. The plate separations are 100 nm.

TABLE III. Attenuation (α dB/μm) of graphene-graphene PPWG with d = 100 nm.

f (GHz)		10	100	250	500	750	1000	1500	2000
Gr-Gr $B_0 = 0$	$\mu_c = 0.2$ eV	0.2628	0.771	1.0824	1.2825	1.3553	1.3844	1.3984	1.3932
	$\mu_c = 0.5$ eV	0.1663	0.4885	0.6866	0.8151	0.8632	0.8836	0.8963	0.8967
Gr-Gr $B_0 = 1$ T	$\mu_c = 0.2$ eV	0.4172	1.3164	2.0185	2.5107	2.5501	2.4006	2.0319	1.7819
	$\mu_c = 0.5$ eV	0.187	0.5636	0.8128	0.9594	0.9823	0.9731	0.9467	0.9276
Gr-Gr $B_0 = 5$ T	$\mu_c = 0.2$ eV	1.5799	5.1852	8.5155	11.867	13.569	14.331	14.418	13.49
	$\mu_c = 0.5$ eV	0.454	1.4872	2.405	3.2254	3.4895	3.4134	2.7554	2.034

Using Eq. (14) it is possible to derive the roots of the dispersion equation. Fig. 6 illustrates the roots β/k_0 of the dispersion relation as a function of frequency for plate separations of d = 100 nm with and without magnetic field bias. The attenuation of this waveguide is presented in Table III.

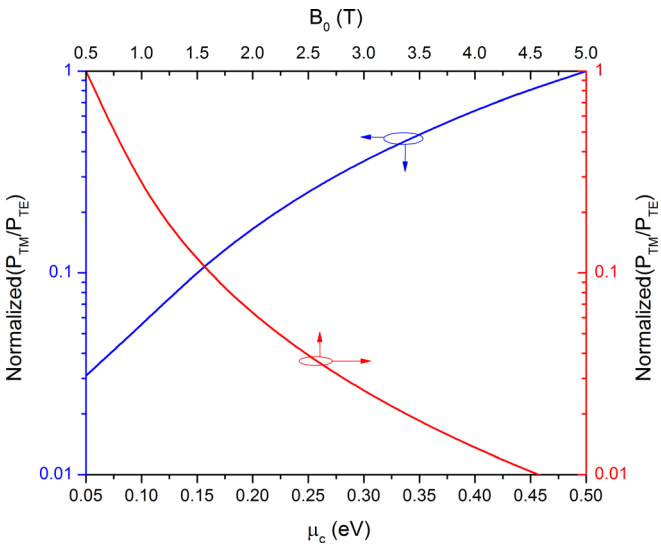

FIG. 7. The proportion of time average power in TE and TM modes for graphene-graphene as a function of the chemical potential (gate voltage V_G) and bias magnetic field at $f = 100$ GHz and for d = 100 nm.

As discussed before, one can control the wave propagation characteristics inside the graphene based waveguides. Regarding Eq. (12), the power proportion of TE and TM modes along the z axis is calculated and depicted in Fig. 7, where we have varied either the electric or magnetic bias leaving the other constant. In the B_0 constant condition ($B_0 = 1$ T), the $P_{avg(TM)}/P_{avg(TE)}$ decreases with increasing the gate voltage. In the constant chemical potential condition $\mu_c = 0.2$ (equivalent to constant voltage bias), the $P_{avg(TM)}/P_{avg(TE)}$ increases as the applied magnetic field is increased.

IV. CONCLUSION

We have investigated the wave propagation characteristics inside parallel plate waveguides with either PEC-graphene or graphene-graphene plates. In the presence of a magnetic field bias, the Maxwell equations' solution inside the waveguide shows that hybrid TM and TE modes exist. We show that wave propagation characteristics can be modified by the externally applied electric and magnetic field biases. The confinement of the field can be improved by reducing the plate separation, increasing the permittivity of the dielectric layer, or increasing the electric bias field. The demonstrated capabilities of graphene based waveguides should find promising applications in transmission lines, filters, and antennas. To our knowledge, we are the first to report these results. The presented analytical procedure is

applicable to other guiding structures having walls with isotropic or anisotropic conductivities.

[1]K. S. Novoselov, A. K. Geim, S. V. Morozov, D. Jiang, Y. Zhang, S. V. Dubonos, I. V. Grigorieva, and A. A. Firsov, "Electric field effect in atomically thin carbon films," Science **306**, 666–669 (2004).

[2]A. K. Geim and K. S. Novoselov, "The rise of graphene," Nature Mater. **6**, 183–191 (2007).

[3]K. S. Novoselov, D. Jiang, F. Schedin, T. Booth, V. V. Khotkevich, S. V. Morozov, and A. K. Geim, "Two dimensional atomic crystals," Proc. Natl. Acad. Sci. U.S.A. **102**, 10451–10453 (2005).

[4]K. S. Novoselov, A. K. Geim, S. V. Morozov, D. Jiang, M. I. Katsnelson, I. V. Grigorieva, S. V. Dubonos, and A. A. Firsov, "Two-dimensional gas of massless dirac fermions in graphene," Nature Lett. **438**, 197–200 (2005).

[5]K. S. Kim *et al*., "Large-scale pattern growth of graphene films for stretchable transparent electrodes," Nature Lett.**457**, 706–710 (2009).

[6]G. Deligeorgis *et al*., "Microwave propagation in graphene," Appl. Phys. Lett. **95**, 073107 (2009).

[7]G. Deligeorgis *et al*., "Electromagnetic propagation in graphene in the mm-wave frequency range," in *Proceedings of the 5th European Microwave Integrated Circuits Conference, Paris* (2010), pp. 1619–1622.

[8]A. Vakil and N. Engheta, "Transformation optics using graphene," Science **332**, 1291–1294 (2011).

[9]F. Bonaccorso, Z. Sun, T. Hasan, and A. C. Ferrari, "Graphene photonics and optoelectronics," Nat. Photonics **4**, 611–622 (2010).

[10]H. S. Skulason, H. V. Nguyen, A. Guermoune, V. Sridharan, M. Siaj, C. Caloz, and T. Szkopek, "110 GHz measurement of large-area graphene integrated in low-loss microwave structures," Appl. Phys. Lett. **99**, 153504 (2011).

[11]M. Dragoman, D. Neculoiu, A. Cismaru, A. A. Muller, G. Deligeorgis, G. Konstantinidis, D. Dragoman, and R. Plana, "Coplanar waveguide on graphene in the range 40 MHz–110 GHz," Appl. Phys. Lett. **99**, 033112 (2011).

[12]G. W. Hanson, "Dyadic Green's functions and guided surface waves for a surface conductivity model of graphene," J. Appl. Phys. **103**, 064302 (2008).

[13]G. W. Hanson, "Dyadic Green's functions for an anisotropic, non-local model of biased graphene," IEEE Trans. Antennas Propag. **56**(3), 747–757 (2008).

[14]G. W. Hanson, "Quasi-transverse electromagnetic, modes supported by a graphene parallel-plate waveguide," J. Appl. Phys. **104**, 084314 (2008).

[15]G. W. Hanson, A. B. Yakovlev, and A. Mafi, "Excitation of discrete and continues spectrum for a surface conductivity model of graphene," J. Appl. Phys. **110**, 114305 (2011).

[16]S. A. M. Abadi, S. Charlebois, and D. Deslandes, "Hybrid modes propagation inside parallel plate waveguide using anisotropic graphene plate," in *IEEE MTT-S International Microwave Symposium Digest, Montréal, QC, Canada*, June 2012, pp. 1–3.

[17]V. P. Gusynin, S. G. Sharapov, and J. P. Carbotte, "Magneto-optical conductivity in graphene," J. Phys. Condens. Matter **19**, 026222 (2007).

[18]V. P. Gusynin and S. G. Sharapov, "Transport of Dirac quasiparticles in graphene: Hall and optical conductivities," Phys. Rev. B **73**, 245411 (2006).

[19]V. P. Gusynin, S. G. Sharapov, and J. P. Carbotte, "Unusual microwave response of Dirac quasiparticles in graphene," Phys. Rev. Lett. **96**, 256802 (2006).

[20]D. M. Pozar, *Microwave Engineering*, 3rd ed. (Wiley, 2005).

[21]I. Crassee, J. Levallois, A. L. Walter, M. Ostler, A. Bostwick, E. Rotenberg, T. Seyller, D. van der Marel, and A. B. Kuzmenko, "Giant faraday rotation in single- and multilayer graphene," Nature Phys. **7**, 48–51 (2011).

[22]Y. Zhang, Y.-W. Tan, H. L. Stormer, and P. Kim, "Experimental observation of the quantum Hall effect and Berry's phase in graphene," Nature Lett. **438**, 201–204 (2005).

[23]V. W. Brar, Y. Zhang, Y. Yayon, T. Ohta, J. L. McChesney, A. Bostwick, E. Rotenberg, K. Horn, and M. F. Crommie, "Scanning tunneling spectroscopy of inhomogeneous electronic structure in monolayer and bilayer graphene on SiC," Appl. Phys. Lett. **91**, 122102 (2007).

[24]S. Marchini, S. Günther, and J. Wintterlin, "Scanning tunneling microscopy of graphene on Ru(0001)," J. Phys. Rev. B **76**, 075429 (2007).

[25]C. H. Lui, L. Liu, K. F. Mak, G. W. Flynn, and T. F. Heinz, "Ultra flat graphene," Nature Lett. **462**, 339–341 (2009).

[26]R. Decker, Y. Wang, V. W. Brar, W. Regan, H.-Z. Tsai, Q. Wu, W. Gannett, A. Zettl, and M. F. Crommie, "Local electronic properties of graphene on a BN substrate via scanning tunneling microscopy," Nano Lett. **11**, 2291–2295 (2011).

[27]M. Walther, D. G. Cooke, C. Sherstan, M. Hajar, M. R. Freeman, and F. A. Hegmann, "Terahertz conductive of thin gold films at the metal insulator percolation transition," Phys. Rev. **76**, 125408 (2007).

[28]R. F. Harrington, *Time-Harmonic Electromagnetic Fields* (McGraw-Hill, New York, 1961), Chap. 7.